Model-based analysis of myocardial strain data acquired by tissue Doppler imaging

Le Rolle Virginie [1 *] **, Hernandez Alfredo I.** [1] **, Richard Pierre-Yves** [2] **, Donal Erwan** [1 3] **, Carrault Guy** [1]

[1] *LTSI, Laboratoire Traitement du Signal et de l'Image INSERM : U642, Université de Rennes I, Campus de Beaulieu, 263 Avenue du Général Leclerc - CS 74205 - 35042 Rennes Cedex,FR*

[2] *IETR, Institut d'Electronique et de Télécommunications de Rennes CNRS : UMR6164, Université de Rennes I, Institut National des Sciences Appliquées de Rennes, SUPELEC, Campus de Beaulieu Bâtiment 11D 35042 Rennes Cedex,FR*

[3] *Département de cardiologie et maladies vasculaires CHU Rennes, Hôpital Pontchaillou, Université de Rennes I, 2 rue Henri Le Guilloux 35033 RENNES cedex 9,FR*

* Correspondence should be adressed to: Virginie Le Rolle <virginie.lerolle@univ-rennes1.fr>

Abstract

Summary

Objective

Tissue Doppler Imaging (TDI) is commonly used to evaluate regional ventricular contraction properties through the analysis of myocardial strain. During the clinical examination, a set of strain signals is acquired concurrently at different locations. However, the joint interpretation of these signals remains difficult. This paper proposes a model-based approach in order to assist the clinician in making an analysis of myocardial strain.

Methods and material

The proposed method couples a model of the left ventricle, which takes into account cardiac electrical, mechanical and hydraulic activities with an adapted identification algorithm, in order to obtain patient-specific model representations. The proposed model presents a tissue-level resolution, adapted to TDI strain analysis. The method is applied in order to reproduce TDI strain signals acquired from two healthy subjects and a patient presenting with Dilated Cardiomyopathy (DCM).

Results

The comparison between simulated and experimental strains for the three subjects reflects a satisfying adaptation of the model on different strain morphologies. The mean error between real and synthesized signals is equal to 2.34% and 2.09%, for the two healthy subjects and 1.30% for the patient suffering from DCM. Identified parameters show significant electrical conduction and mechanical activation delays for the pathologic case and have shown to be useful for the localization of the failing myocardial segments, which are situated on the anterior and lateral walls of the ventricular base.

Conclusion

The present study shows the feasibility of a model-based method for the analysis of TDI strain signals. The identification of delayed segments in the pathologic case produces encouraging results and may represent a way to better utilize the information included in strain signals and to improve the therapy assistance.

MESH Keywords Case-Control Studies ; Echocardiography, Doppler ; methods ; Heart Ventricles ; Humans ; Models, Theoretical

Author Keywords
Index Terms
Biomedical systems modeling ; Biomedical model simulation ; Model-based interpretation ; Echocardiography

Introduction

In the daily clinical practice, Doppler Echocardiography has become a fundamental method in evaluating the cardiac function. This non-invasive technique is particularly useful for the analysis of blood flow and cardiac anatomy, facilitating the diagnosis of cardiovascular pathologies. Tissue Doppler Imaging (TDI) is a more recent tool that can be useful in assessing regional myocardial deformations through the estimation of regional myocardial strain [1, 2] and strain rate [3]. Myocardial strain analysis has shown to be useful, for example, in differentiating healthy and ischemic myocardium [4, 5]. More details on TDI acquisition and analysis are presented in appendix A.

A typical experimental strain signal is shown in figure 1. Tissue extensions correspond with positive strains while tissue compressions result in negative strains. This signal reflects the different phases occurring during the cardiac cycle (figure 1): i) the isovolumic contraction phase; ii) the systole; iii) the isovolumic relaxation; iv) the diastole, which can be divided into three periods: the first one

corresponding to a rapid filling phase due to an aspiration of blood inside the ventricle, a slower filling period and the late diastolic filling phase, corresponding to the atrial systole.

Although TDI presents some disadvantages such as a dependence on the ultrasound beam orientation [1], that affects the reproducibility, and the presence of noise [2], it has been successfully validated by the comparison with other imaging methods, like MRI or sonomicrometry [2, 6]. The main advantages of TDI are related to the possibility of obtaining real-time measurements and the relative low cost of this technique.

Several indicators can be derived from strain estimations, such as maximum systolic velocity or ventricular filling period [4, 7]. Although the use of such indicators has already shown interesting results in identifying some cardiovascular pathologies, the whole information contained in the strain signal is not yet fully utilized.

The analysis of the morphology of a set of strain signals, acquired concurrently at different regions of the myocardium, is a very difficult task. This is partly due to the multidimensionality of the problem and the fact that the different processes which lead to ventricular contraction (mechano-hydraulic interactions, electrical activation and propagation, etc.) have to be jointly considered for an appropriate interpretation.

In this paper we propose a model-based approach to assist the clinician on the analysis of myocardial strain signals. A brief presentation of current approaches for modeling the electromechanical activity of the heart is proposed in section 2. Section 3 describes the proposed ventricular model and the parameter identification method. Finally, in section 4, the results of patient-specific identifications and the analysis of strain morphologies are presented and discussed.

Current electromechanical models of the cardiac function

A variety of mathematical models of the ventricular function have been proposed in other studies. The simplest models are based on a time-varying elastance [8, 9]. These overall, lumped-parameter models give realistic simulations of cardiac pressure and volume and require low computational resources. However, as the whole left ventricle (LV) is represented as a single element, it is not possible to analyze the regional ventricular function. Other approaches have been proposed in order to represent explicitly, at many different levels of detail, the cardiac electrical activity, the excitation-contraction coupling, the mechanical activity and the mechano-hydraulic coupling. The main modeling techniques applied to represent these activities are briefly recalled in the following paragraph.

Electrical Activity

Models of the cardiac electrical activity, defined at the cell level, can be classified into three categories:

- Biophysical continuous models, composed of detailed descriptions of the cardiac action-potential, based on the Hudking-Huxley formulation [10], and presenting different levels of detail on the ionic currents included [11–13].

- Phenomenological continuous models, which reproduce qualitatively the electrical activation without describing the different ion channels. They present less computational requirements and result in simplified representations of the model's electrical activity (often based on the FitzHugh- Nagumo model [14]).

- Simplified discrete models, they are often based on cellular automata, representing the different electrical states of a myocyte's action potential [15].

Coupling of cell-level continuous models in order to represent a patch of myocardial tissue, or more complex geometries such as the whole LV, can be performed by using the monodomain or bidomain approaches [16, 17]. Cellular automata are typically coupled by means of a discrete flag transmitted to all neighbors during the depolarization of each element [18]. Another approach to represent the propagation of the cardiac electrical activity is limited to modeling the evolution of the depolarization wavefront through the cardiac tissue, described by the eikonal diffusion equation [19].

Mechanical Activity

The ventricular mechanical activity is usually described as a function of its active and passive properties. Active properties are the consequence of the shortening and lengthening of sarcomeres, which are the elementary mechanical contractile elements of myocytes. This mechanical activity is under the influence of an electrical activity, since the variation of calcium concentration during the action potential allows the development of force. Passive properties are mainly related to fiber structure and orientation, collagen properties and metabolic conditions (such as hypoxia or ischemia).

Models of the active properties include:

- Huxley-type models, which represent changes of conformation on sarcomeres as a function of cross-bridge position [20] and intracellular calcium concentration [21].

- Hill's models, which use one of the forms of the original Hill's force-length relation [22–24] or the modified Hill equation, which is a sigmoid function relating calcium concentration and active tension.

- The HMT model, proposed by Hunter–McCulloch–ter Keurs [25], which includes a rather detailed description of protein kinetics associated with myofilament length modifications.

- Phenomenological approaches, which are based on time-varying analytical activation functions that reach their minimum during diastole and their maximum during systole. A number of such analytical functions have been proposed, with different forms and parameters, such as in [26, 27].

Passive myocardial properties are mainly described through specific mechanical constitutive laws. Most of these mechanical laws are hyperelastic, incompressible and anisotropic [28–30]. The majority of them have been determined using uniaxial [31] or biaxial tension tests [30]. An empiric law based on the description of sarcomere dynamics has been proposed by [22].

The simulation of these models are often based on finite-element methods (FEM) [32–35]. Although this kind of formulation allows a rather detailed description of the myocardium dynamics, it requires significant computational resources. Another complementary approach for modeling the myocardium deformation is based on a mass-spring system [36] activated by a model of the electrical activity through a simplified electro-mechanical coupling.

Fluid-structure interaction and boundary conditions

The simulation of a realistic cardiac cycle requires the representation of the interaction between the myocardium and the blood inside the heart's chambers and in the systemic and pulmonary circulations. Several approaches to this have been proposed:

- Fluid-structure interaction models integrate simultaneous descriptions of the fluid inside the cavity, by means of a Navier-Stokes formulation [37, 38] and the myocardial wall motion, based on the description of a constitutive law, as presented in the previous section.

- Rule-based definition of boundary conditions: In most FEM models of the LV, boundary conditions are imposed by the intra-ventricular pressure, by means of a set of rules defining different levels of pressure for each phase of the cardiac cycle. The ejection and filling phase can be deduced from a simplified model of the circulation [32, 34], while a penalty pressure is applied during the isovolumetric phases, in order to keep the volume constant [39]. An alternative method has been proposed in a recent paper, combining a lumped parameter model of the circulation with an FEM model of the ventricles, based on the estimation of an equivalent overall ventricular elastance for each time-step [40]. These approaches imply the uniformity of blood pressure inside the cavity. However, Courtois et al have shown the importance of regional pressure gradients in the LV, especially during diastole [41].

Model-based analysis of strain signals

Complete models of ventricular activity are developed from a combination of the several different approaches previously described and some of these models have been applied to the analysis of myocardial strain. Nickerson et al [42] proposed a 3D model of cardiac electromechanics and used the fiber extension ratio to study the role of electrical heterogeneity in the cardiac function. The model includes a precise description of ventricular contraction, but requires around three weeks of simulation time on a parallel computer in order to reproduce one beat. Kerckhoffs et al [27] have proposed a 3D finite element model of cardiac mechanics used to compare synthesized ventricular strain signals generated by a normal and a synchronous electrical activation sequence. The model simulations show unphysiological contraction patterns when a physiological electrical activation is applied. Results illustrate the difficulty of using such a model in a concrete clinical application and the necessity of representing heterogeneous electromechanical couplings. The same model has been used by Ubbink et al [43] to study circumferential and circumferential-radial shear strain. Simulated strains are compared to Magnetic Resonance Tagging (MRT) data. The model-based approach helps in determining the influence of fiber angle on regional contraction. However, as the model includes simplified descriptions of its hydraulic activity, the whole morphology of ventricular strain cannot be analyzed, especially during the rapid filling phases.

As previously stated, the main objective of this study is to propose a personalized model-based approach in order to assist the clinicians in the interpretation of myocardial strain signals measured with Tissue Doppler echocardiography. The models described in the previous paragraphs are difficult to apply in this case, as they are characterized by a significant number of parameters, require significant computational resources and, consequentially, their ability to be identified is more complex. Previous studies [44] have shown the benefit of combining a minimal cardiovascular model and an identification algorithm for real-time patient specific modeling and diagnosis in the case of a pulmonary embolism. As the high resolution of an FEM model is not necessary for this particular study, a new model has thus been developed, with the following specific properties:

- The model resolution has been adapted to the problem, keeping a similar abstraction level as the experts for the analysis of strain signals.

- The model is based on a functional integration of interacting physiological processes, by taking into account: i) the electro-mechanical coupling, ii) the interactions between the myocardial wall and the blood inside the cavity and iii) a simplified representation of the systemic circulation. This allows the representation of the main cardiac properties required to tackle the problem under study, like the Frank-Starling law and the influence of preload and afterload.

The next section presents a detailed description of the proposed model and the identification algorithm which is applied in order to obtain patient-specific model parameters.

Materials and methods

Model description

General presentation of the proposed model

In order to simulate the strain measured for each myocardial region, the proposed LV model has been divided into twelve segments, composed of three layers at the basal, equatorial and apical level [45]. Each layer is separated into 4 components: septal, lateral, anterior and inferior wall (figure 2). Each wall segment interacts with the blood inside the corresponding intra-ventricular cavity (which is itself segmented in a consistent manner). It should be noticed that such a 12-wall segmentation does not correspond to the standard myocardial segmentation defined in [46]. However, this segmentation has already been used in different studies (such as in [45]) and remains significant from a clinical standpoint.

The LV has been approximated by a truncated ellipsoid as it has already produced encouraging results in other studies, for the analysis of the electrical propagation during contraction [19, 47] or ventricular torsion [48]. The choice concerning the modeling formalism for each cardiac activity are summarized here:

- Electrical activity: A cellular automata network has been chosen to describe the electrical activation sequence for the 12 segments. This formalism presents low computational costs, while describing the basic properties of the cardiac electrical activity.

- Mechanical activity: The myocardium has been supposed to be hyperelastic, incompressible and transverse isotropic. The twist motion of the ventricle has been neglected, as it cannot be measured with tissue Doppler echocardiography. As circumferential and longitudinal strains are less sensitive to cardiac fiber angle [43], only a mean fiber angle is taken into account.

- Hydraulic activity: A lumped parameter model is used to describe the hydraulic activity of the intra-ventricular cavity and the influence of preload and afterload. This representation is adapted to reproduce major cardiac properties like the Frank-Starling law and the representation of regional pressure gradient that has been observed in the LV [41].

The proposed model can be seen as an improvement of elastance models, by representing a set of sub-pumps interconnected in the hydraulic domain and commanded by a coordinated electrical activity. Each pump represents a macroscopic, tissue-level segment of the LV wall.

Electrical activation model

The ventricle has been represented by twelve cellular automata to describe the electrical propagation during contraction. Each automaton is defined by four electrical states [49, 50] (figure 3): i) rapid depolarization period (RDP), ii) absolute refractory period (ARP), iii) relative refractory period (RRP) and iv) a waiting period (idle). The transitions between states happen spontaneously at the end of the duration of each phase or due to an external activation, during the idle or RRP states. After the RDP period, each automaton transmits a stimulus to its neighboring segments. Each automaton is fully connected (antegrade and retrograde connections) to its three or four neighbors. An external excitation first stimulates the mid-septum segment and is then propagated to the other segments in function of each automaton's parameter values.

Electrical activation has been described as an anisotropic propagation [51], as the conduction delay is about three times longer in the horizontal direction than in the vertical direction. The coupling between two cellular automata is defined by the period T_1 for the antegrade link and the period T_2 for the retrograde link (see figure 3). For a vertical coupling, these periods are defined as $T_1 = Trdp_1$ and $T_2 = Trdp_2$. For a horizontal coupling, they are equal to $T_1 = 3.Trdp_1$ and $T_2 = 3.Trdp_2$.

Mechanical–hydraulic model

The radial force developed by each segment is computed by integrating the radial stress on the wall surface. Myocardial stress is usually expressed as the sum of active and passive stresses.

$$F_r = \int \sigma_r \cdot dS = \int (\sigma_{ra} + \sigma_{rp}) \cdot dS$$

The active stress can be expressed using the relation:

$$\sigma_a = T_a \cdot (FN) \cdot (FN)^T$$

where F is the deformation gradient tensor, N stands for a unitary vector in the fiber direction and T_a is the active tension. As in other studies [26, 27], T_a is approached by means of a trigonometric function. In this case, the T_a function is inspired from the studies of Hunter et al [25] and is defined as:

$$T_a = T_{ref} \frac{[Ca^{2+}]_i^n}{[Ca^{2+}]_i^n + Ca_{50}^n} [1 + \beta(\lambda - 1)]$$

where T_{ref} is the value of the tension at $\lambda = 1$, Ca_{50} the calcium concentration at 50% of the isometric tension, n is the Hill coefficient determining the shape of the curve and β is the myofilament "cooperativity". The parameters values and functions for Ca_{50} and n are taken from [25]. $[Ca^{2+}]_i$ is the intracellular calcium concentration, which represents the mechanical activation level, and is defined in this model as:

$$[Ca^{2+}]_i = \begin{cases} 0 & t_{es} < 0 \\ K \sin(\pi \cdot t_{es} / T_{\max}) & 0 \le t_{es} \le T_{\max} \\ 0 & t_{es} > T_{\max} \end{cases}$$

Where t_{es} is the time elapsed since the end of the RDP for each segment s, T_{max} the activation duration and K the maximum level of calcium concentration. The deformation gradient tensor F can be defined by characterizing the myocardial motion in spherical coordinates. Supposing that a material particle in the undeformed state (R,Θ,Ψ) goes to (r,θ,ϕ) in the deformed state, a radial deformation can be described by:

$$r = r(R); \quad \theta = \Theta; \quad \phi = \Psi$$

These relations define a square diagonal matrix F that includes the strains λ_r , λ_θ and λ_ϕ in the three principal directions. It can easily be shown that the deformations in these directions are expressed as: $\lambda_r = \partial r/\partial R$ and $\lambda_\theta = \lambda_\phi = r/R$, the latter common value being usually denoted by λ. Additionally, the myocardium is supposed to be incompressible, which is a classical assumption for the cardiac muscle, and the following additional property holds: $\det(F) = 1$. So a simple relation between λ_r and λ can be found: $\lambda_r = 1/\lambda^2$.

The passive stress is due to myocardium organization (fibers, collagen…) and can be expressed using the equation:

$$\sigma_p = -pI + 2F \frac{\partial W}{\partial C} F^T$$

where W is the strain energy function, p stands for the hydrostatic pressure, I is the identity matrix and C is the Cauchy-Green tensor computed from F through $C = F^T F$. The energy function used in this paper is the one defined by Humphrey et al. [28], which is a polynomial energy function. The polynomial form facilitates the implementation and has shown its efficiency in many studies [48, 52]:

$$W = c_1(\alpha - 1)^2 - c_2(\alpha - 1)^3 + c_3(I_1 - 3) + c_4(I_1 - 3)(\alpha - 1) + c_5(I_1 - 3)^2$$

Where I_1 and $\alpha = \sqrt{I_4}$ stand for the invariants of the deformation gradient tensor. Finally, the passive stress can be expressed as:

$$\sigma_p = -pI + 2W_1 B + 2W_4 FN \times NF^t$$

with $W_1 = \partial W/\partial I_1$, $W_4 = \partial W/\partial I_4$, $I_1 = \mathrm{tr}(C)$ and $I_4 = N^t .C.N$

Since the total stress tensor has been defined as the sum of the active and passive ones, the three directions components are:

$$\sigma_r = -p + \tilde{\sigma}_r$$
$$\sigma_\theta = -p + \tilde{\sigma}_\theta$$
$$\sigma_\phi = -p + \tilde{\sigma}_\phi$$

$$\text{where } \tilde{\sigma}_r = 2 \cdot W_1 / \lambda^4,$$
$$\tilde{\sigma}_\theta = 2 \cdot W_1 \cdot \lambda^2 + 2 \cdot W_4 \cdot \lambda^2 \cdot \cos(\psi) + T_a \cdot W_4 \cdot \lambda^2 \cdot \cos(\psi)$$
$$\tilde{\sigma}_\phi = 2 \cdot W_1 \cdot \lambda^2 + 2 \cdot W_4 \cdot \lambda^2 \cdot \sin(\psi) + T_a \cdot W_4 \cdot \lambda^2 \cdot \sin(\psi)$$

This equation system is implicit and the Laplace Relation is added to link the three stress components. This relation has been demonstrated for a thin ellipsoidal myocardial segment in [53], which shows that the thin wall theory is adequate for the estimation of average longitudinal and latitudinal stresses in ventricular walls:

$$-\sigma_r = \frac{\sigma_\theta \times e}{R_\theta} + \frac{\sigma_\phi \times e}{R_\phi}$$

where e is the wall thickness, R_ϕ and R_θ stand for the radii of curvature in the meridian and parallel directions. As the ventricle is assumed to be an ellipsoid of revolution, (R_ϕ , R_θ) can be expressed as:

$$R_\phi = \frac{(a^2 \cdot \cos^2\phi + b^2 \cdot \sin^2\phi)^{3/2}}{ab}$$
$$R_\theta = \frac{a}{b}(a^2 \cdot \cos^2\phi + b^2 \cdot \sin^2\phi)^{1/2}$$

Since σ_r can be computed, the wall radial force can be obtained by integrating the radial stress on the segment surface:

$$F_r = -\int \sigma_r dS = \tilde{\sigma}_\theta \cdot \lambda^2 \cdot K_\theta + \tilde{\sigma}_\phi \cdot \lambda^2 \cdot K_\phi - \tilde{\sigma}_r \cdot \lambda^2 \cdot K_r$$

with

$$\frac{\sin\phi}{\frac{R_\phi}{e} + \frac{R_\phi}{R_\theta}} \cdot d\phi \cdot d\theta, \quad K_\phi = \iint \frac{R^2 \sin\phi}{1 + \frac{R_\phi}{e} + \frac{R_\phi}{R_\theta}} \cdot d\phi \cdot d\theta, \quad K_r = \iint \frac{e \cdot R_\phi + e \cdot R_\theta}{e \cdot R_\phi + e \cdot R_\theta + R_\phi \cdot R_\phi} \cdot R^2 \cdot s$$

This last relation provides the constitutive law suitable to model the segment.

Mechano-Hydraulic coupling

The mechano-hydraulic interaction between the myocardial wall and the blood inside the ventricular cavity is characterized by the coupling relation:

$$P_S = \frac{F_r}{S}$$

where P_S is the pressure on the wall surface, F_r is the radial force developed by the wall segment and S can be easily calculated since the surface is ellipsoidal.

Hydraulic description

The blood behavior inside the cardiac cavity should also be described. Indeed, although the flow Q is supposed to remain the same in each cavity segment, the pressure varies from the wall surface (P_S) to the cavity center (P_c). This variation is partially due to blood viscosity. So a hydraulic resistance R is defined. To describe the rapid filling phases, this resistance is considered lower during the diastole (R_{min}) and higher during systole (R_{max}). A resistive law relates pressure and flow:

$$Q = \frac{P_c - P_s}{R}$$

It is also necessary to take into account the blood mass effects which bring some inertial properties. So a hydraulic inertance I can be introduced in order to define the law:

$$P_c - P_s = I\frac{dQ}{dt}$$

To summarize, each ventricular segment is modeled by four distinct entities for the electrical, mechanical, mechano-hydraulic coupling and hydraulic parts. Each part is composed of the equations previously described and some input-output relations. The links between the different parts of the segment model are graphically described in figure 4.

Segments are also connected through the hydraulic domain (figure 5) as the total flow Q_t is the sum of the regional flows Q_i :

$$Q_t = \sum_i Q_i$$

The connections between the three layers are defined by considering the resistive properties of the blood inside the cavity.

The preload has been modeled by a constant flow source connected to a time-varying elastance that describes the atrial behavior [54]:

$$E_a = \begin{cases} \frac{E_{\max} - E_{\min}}{2}(1 - \cos(\frac{\pi \cdot t_{ea}}{T_{\max}})) + E_{\min} & 0 \le t_{ea} \le 2 \cdot T_{\max} \\ E_{\min} & 2 \cdot T_{\max} \le t_{ea} \le T \end{cases}$$

where t_{ea} corresponds to the time elapsed since atrial electrical activation. The afterload is described by a Windkessel model composed of a capacity, a resistance and an inertance. The heart valves are represented by non-ideal diodes that correspond to modulated resistances and the valvular plane is described by a linear capacitance.

In summary, the ventricular model is based on an ellipsoidal geometry and is composed of twelve segments which describe the different energy domains involved in cardiac function: i) the electrical activity is described by a cellular automata network, ii) the mechanical-hydraulic model represents the influence of both active and passive forces developed by each segment on the blood inside the cardiac cavity. The twelve segments are differentiated by specific parameters characterizing their electrical and mechano-hydraulic properties.

The values for most of the parameters describing the mechanical behavior (c1, c2, c3, c4, c5, Tref, Bo, B1, nref, pC50ref, B2) have been taken from other studies [25, 52]. The parameter values controlling afterload and preload (capacitance, resistance, inertance and elastance) have been taken from [54, 55]. Appendix B presents all these parameter values. The other parameters values are determined by means of the identification algorithm. These parameters include the mechanical activation period (T_{max}), the maximum activation level (K) and the RDP period, for each segment.

Figure 6 presents the simulation of overall hemodynamic variables: ventricular pressure, flow and volume for a normal cardiac cycle. Parameters for cellular automata have been fixed to fit electrical activation patterns from [51]. The activation duration is equal to 400ms [26] and the maximum level of calcium concentration is fixed at 7 μM [27].

Figure 7 shows simulated strains in basal and equatorial segments for a normal and a pathologic case. The simulation of one cardiac cycle (800 ms of simulation), takes about 20s on a dual-core Intel Xeon 2.66Ghz.

The normal case (figure 7A) is simulated by using the same parameters as those used in figure 6. A pathologic condition has been simulated by applying an additional electrical activation delay of 50 ms to the anterior basal segment (figure 7B). The consequences of this regional desynchronisation can be observed on the simulated strains during the isovolumic contraction phase, as the normal activation of the other myocardial segments has produced an extension of the delayed segment. This phenomenon is marked with a circle in figure 7B.

Model adaptation to experimental data

The model-based process, which is applied to the interpretation of strain morphology, is presented in figure 8. The whole process is composed of three main steps: i) acquisition of strain signals measured by TDI, ii) adaptation of the model's geometrical shape to real dimensions, determined by echocardiography and the identification of patient-specific parameter values to reproduce the observed strain and iii) the physiological interpretation of the identified parameters. This model-based approach is based on studies completed by our laboratory which led to patient-specific parameter identification methods with applications in cardiology [50] or epileptology [56].

Concerning the adaptation of the geometrical shape, echocardiography reports usually inform us of the ventricle's length (L) and diameter (D). The model's ellipsoid dimensions are defined from this data. In fact, if the diameter is supposed to be measured at the equator, the minor axis can be computed as a = D/2. Additionally, a relation between the major axis and the ventricle length is defined in [57] as b = 2L/3 (figure 9). Since the major and minor axes are known, it is possible to calculate, for each segment, the surface (S) and the radii of curvature in order to get coefficients K_θ , K_ϕ , K_r .

The identification algorithm is used to minimize the difference between experimental and simulated strains on the eight myocardial segments at the base and at the equator. Parameters related to the four apical segments have not been identified, as the strain data from

these segments are difficult to acquire. For these apical segments, the model parameters have been fixed from mean physiological values. These values are listed in appendix 2.

Identification algorithm

The parameter identification can be seen as an optimization problem consisting of minimizing, for each beat i, an error function defined as the difference between the synthesized strains and the observed strains. The synthesized strains are obtained by simulating the proposed model M with a specific set of parameter values P, such that:

$$X_s^{obs} = Strain_s^{obs}(t)$$
$$X_s^{sim} = Strain_s^{sim}(t) = M(P)$$

where X_s^{obs} and X_s^{sim} represent, respectively, the observed and simulated strains for segment s and $t = [\tau_{QRS_i}, \ldots, \tau_{QRS_{i+1}}]$ where τ_{QRS_i} represents the QRS detection instant for beat i.

The parameter set P defines the following values for each segment: the mechanical activation period (T_{max}), the maximum activation level (K) and RDP period ([$RDP_{\_segment}$, $K_{\_segment}$, $T_{\_segment}$]). Additionally, two hydraulic resistance values are determined at the base and the equator ([$R_{\_max\_base}$, $R_{\_min\_base}$, $R_{\_max\_equateur}$, $R_{\_min\_equateur}$]). In total, 28 parameters have to be identified and P is defined as P=[$R_{\_max\_base}$, $R_{\_min\_base}$, $R_{\_max\_equateur}$, $R_{\_min\_equateur}$, $RDP_{\_ant\_base}$, $RDP_{\_inf\_base}$, $RDP_{\_lat\_base}$, $RDP_{\_septum\_base}$, $RDP_{\_ant\_equa}$, $RDP_{\_inf\_equa}$, $RDP_{\_lat\_equa}$, $RDP_{\_septum\_equa}$, $K_{\_ant\_base}$, $K_{\_inf\_base}$, $K_{\_lat\_base}$, $K_{\_septum\_base}$, $K_{\_ant\_equa}$, $K_{\_inf\_equa}$, $K_{\_lat\_equa}$, $K_{\_septum\_equa}$, $T_{\_ant\_base}$, $T_{\_inf\_base}$, $T_{\_lat\_base}$, $T_{\_septum\_base}$, $T_{\_ant\_equa}$, $T_{\_inf\_equa}$, $T_{\_lat\_equa}$, $T_{\_septum\_equa}$]. The objective is thus to obtain an optimal set of patient-specific parameters P* which minimize an error function between X_s^{obs} and X_s^{sim}. This error function has been defined here as the sum of the absolute values of the difference between each experimental and simulated strain, calculated for the whole cardiac cycle and for the 8 basal and equatorial segments.

$$\epsilon = \sum_{s=1}^{8} \sum_{t=\tau_{QRS_i}}^{\tau_{QRS_i+1}} \left| Strain_s^{sim}(t) - Strain_s^{obs}(t) \right|$$

This error function is not differentiable and can have multiple local optima. This kind of problem can be solved using Evolutionary Algorithms (EA), which are an adapted method used in identifying complex nonlinear problems characterized by a poorly-known state-space. EA are stochastic search techniques, inspired by the theories of evolution and natural selection, which can be employed to find an optimal configuration for a given system within specific constraints [58].

In these algorithms, the set of parameters P characterizes each “individual” of a “population”. In order to reduce the search space, values for parameters were bounded to the physiologically plausible intervals: [0.5 5] for the maximum hydraulic resistances, [0.01 0.5] for the minimum hydraulic resistances, [0.3 0.9] for calcium period, [5 12] for calcium amplitude and [1 500] for electrical time activation. These intervals have been defined around parameter values used for the simulation of global hemodynamic variables in section 3.1.5 (taken from other studies) and are based on physiological knowledge on the electromechanical activities of the heart.

An initial population is created from a set of randomly generated individuals. The 28 parameter values of a given individual are independently generated from a uniform distribution, defined under the corresponding feasibility interval. This population will “evolve”, minimizing the error function, by means of an iterative process (figure 10).

Once the error function has been evaluated for each individual, a new generation is produced by applying mutation and crossover operators on selected individuals. The selection is carried out by means of the “roulette wheel” method, adapted for function minimization, in which the probability of selecting a given individual depends on the value of its error function, divided by the sum of all the error values of the population. Only standard genetic operators, defined for real-valued chromosomes, have been used in this work: “uniform crossover” , which creates two new individuals (offspring) from two existing individuals (parents), by randomly copying each allele from one parent or the other, depending on a uniform random variable and “Gaussian mutation”, which creates a new individual by randomly changing the value of one allele (selected randomly), based on a Gaussian distribution around the current value. More details on these kinds of optimization methods can be found on [59–61].

Results and Discussion

Acquisition protocol

Strain acquisition using color tissue Doppler imaging has been applied to two healthy subjects and one patient affected with dilated cardiomyopathy (DCM). This pathology is characterized by a heart enlargement and a reduced mechanical cardiac function. Ultrasound measurements were performed in order to determine the LV dimensions on two cardiac cycles.

For the two healthy subjects and the pathologic patient, the minor (a) and major (b) axes values are first determined from echocardiography (Table 1) Dimensions for the pathologic patient are particularly high, which is coherent with the diagnosis of a DCM.

Comparison between simulated and experimental strain

Strain signals have been measured on eight segments of the myocardial wall at the base level (the septum and the anterior, inferior and lateral wall) and the equatorial level (the septum and the anterior, inferior and lateral wall). In fact, it is not possible to obtain accurate data on the apical segments using TDI. Figure 11 shows simulations obtained after parameter adaptation and the clinically recorded strain signals for the three subjects under study. The mean error value (calculated on the eight segments as presented in equation 21) is equal to 2.4%, 2.09% and 1.30% respectively for the two healthy subjects and the pathologic patient, despite the important disparity on the data from each subject.

Simulated systolic peak times are coherent with the observation and the reproduction of the overall morphology of the isovolumic contraction and systolic phases is approached with relative errors of 2.12%, 2.16% and 1.25% for the first, second and third subject, respectively. Additionally, the simulations reproduce some particularities that are due to the pathology. In fact, for the patient suffering from DCM, positive values on some strain signals can be observed during the isovolumic contraction. These strain elevations are due to increased electrical activation delays in the corresponding segments and they can be explained by the extension of yet inactivated segments during the contraction of the other segments. This example shows how the model-based approach may assist in the interpretation of myocardial strain morphologies.

Interpretation of the identified parameters

The previous results can be represented graphically by visualizing the deformations which have been applied to the twelve myocardial segments at each time step. Simulated strains, obtained using patient-specific parameters, are applied at the center of the corresponding myocardial segment. The cardiac surface deformation is computed using Thin Plate Spline (TPS), which is a generalization of 1-D cubic splines [62].

The surface is represented by a graph on which are defined landmarks (data points). The position of each landmark being known during the whole cardiac cycle, the cardiac surface deformation is computed using TPS interpolation (based on a bending energy, defined as the integral, over all the mesh nodes, of the squares of the second derivatives). Figure 12 shows the ventricular deformation and the identified electrical activity for the three subjects during the cardiac cycle. The electrical activation sequences for the two healthy subjects are coherent with well-known activation maps [51]. It possible to observe a reduced mechanical activity and a delayed electrical activation on the DCM patient. A qualitative evaluation of the three simulated sequences has been performed by a cardiologist. He confirms that simulations correspond to pathophysiologically plausible sequences. The delayed electrical activity observed in the simulation for the DCM patient can be explained by an intra-ventricular desynchronisation, frequently observed in this kind of pathology. A quantitative evaluation of the estimated activation sequence could be performed by acquiring an electrophysiological cartography for each patient. This delicate invasive procedure has not been applied for the patient analyzed in this paper. However, this kind of evaluation will be possible using data acquired on a current clinical protocol running at the Rennes University Hospital.

The identification process brings patient-specific parameters that are interesting to analyze, since they can be representative of the physiopathological state. To facilitate the visualization of these results, the “Bull's eye" representation is used to depict the electro-mechanical parameters identified for each segment (figure 13).

Figure 14 shows the electrical activation times for the three patients. The maximum values reach 54 ms, 67.4 ms and 126 ms for the first and second subjects and the DCM patient, respectively. It is easy to verify that the pathologic patient presents increased electrical activation delays in comparison with well-known activation maps [51].

The mechanical activity peak time T_{MP} can also be analyzed. In order to compare this parameter for the three patients, the identified T_{MP} is expressed as a percentage of the cardiac cycle duration (RR interval):

$$T_{MP\%} = 100 \cdot T_{MP} / RR$$

Figure 15 shows the bull's eye representation of identification results. For the first healthy subject, the mechanical activity peak time goes from 18% to 37% of the RR interval. For the second one, this parameter varies from 21% to 37%. T_{MP} % ranges from 31% to 60% for the affected patient.

The T_{MP} % comparison for both healthy subjects shows similar value ranges. The third patient percentages are higher overall. These values are particularly high for the anterior and lateral segments of the base because they are respectively equal to 60 % and 55 %. The

increased T_{MP} % is a marker of a myocardial dysfunction concerning these two segments. The model-based localization of the delayed segments and the magnitude of the desynchronization for the DCM patient are in accordance with the diagnosis provided by the expert cardiologist. Moreover, the model-based approach provided further insight in the explanation of the observed strain morphologies.

Robustness analysis

In order to test the robustness of the identification method, the algorithm has been repeated ten times on one subject. Figure 16 shows boxplots of the identified T_{MP} parameters. The results of the ten identifications are close enough to show that the parameter interpretation is available from a physiological point of view. Furthermore, it can be seen from these box-plots, and from results in section 4.3, that the identified parameter values do not reach the upper or lower boundaries of the physiological plausible intervals defined in section 3.2.1.

Study Limitations

The main limitations of the proposed approach are related to the hypotheses made to build the ventricular model, the observability of TDI strain analysis, and the current clinical evaluation state.

Concerning the ventricular model, the following hypotheses were made in order to obtain a tissue-level, lightweight model on which we could perform parameter identification from observed strain signals: i) the ventricular torsion motion has been neglected, ii) the mechanical continuity between segments is not always assured, as the ventricle is represented by a set of sub-pumps coupled in the hydraulic domain and commanded by a coordinated electrical activity, iii) the intracellular calcium concentration is approximated by an analytic expression and iv) the myocardial fiber orientation is assimilated to a mean angle. Although these simplifications have a direct consequence on the synthesis of strain signals, in particular during the diastolic period (as discussed above), the authors consider that they are in accordance to the problem under study and the resulting model can already be useful to assist in the interpretation of strain data.

Another limitation concerns the limited observability of the apical segments from strain analyses. As already mentioned, in order to overcome this problem, the model parameters for the apical segments have been fixed from mean physiological values and are not included into the identification process.

Finally, concerning the clinical evaluation of the approach, only a limited number of healthy subjects and DCM patients have been analyzed so far. Although these results are encouraging and show the feasibility of the approach, a larger clinical evaluation is necessary in order to validate the interpretations obtained from this model-based approach.

Conclusion

The present paper described a model-based approach for the analysis of myocardial strain data. The method is based on a tissue-level model of the left ventricle that includes a simplified geometrical representation, a description of the electrical, mechanical and hydraulic activities and a physiological segmentation, which are in accordance to the problem under study. As low computational resources are required for the simulations of the proposed model, the identification of patient-specific parameters becomes feasible.

Patient-specific parameters were obtained for two normal subjects and one patient suffering from DCM. The mean error between observed and synthesized strain signals, after parameter identification, is particularly low (between 1.30% and 2.34%). A qualitative comparison between the results obtained from the proposed model-based approach and a classical TDI analysis has been performed by a cardiologist/echocardiographer (ED). The localization of failing segments and the values and instants of occurrence of the peak systolic strains have shown to be coherent with the clinical analysis. The model also allows a better reproducibility in the estimation of systolic peaks and adds the possibility of estimating electrical activation times, which are difficult to observe experimentally. This appears particularly useful as echocardiographic strain signals are sometimes noisy and challenging to interpret, limiting its large use in routine clinical practice. Recent papers insist on this problem of reproducibility and robustness of the echocardiographic interpretation (PROSPECT study [63] and RETHINQ study [64]).

Moreover, such a patient-specific model-based method can be used to assist the interpretation of strain morphologies and to find, via simulations, the origin of particular strain shapes. The main advantage of this model-based approach with respect to “black-box” approaches, such as neural networks, is that the patient-specific parameters characterizing the model provide a direct physiological interpretation. Due to this property, these model-based approaches can be useful for a better interpretation of the morphology of strain signals and to assist diagnosis and therapy definition.

Current work is directed towards the improvement of the ventricular model and a further clinical evaluation of the proposed approach. In this sense, a clinical protocol including electrophysiological cartography, TDI and multi-slice computer tomography on patients receiving cardiac resynchronization therapy is currently in progress in the Rennes University Hospital (IMOP project).

Ackowledgements:

The authors would like to thank Antoine Simon for his valuable assistance in the exploitation of the visualization tools.

References:

- 1. D'Hooge J , Heimdal A , Jamal F , Kukulski T , Bijnens B , Rademakers F , Hatle L , Suetens P , Sutherland GR Regional strain and strain rate measurements by cardiac ultrasound: principles, implementation and limitations. European Journal of Echocardiography. 1: 154- 70 2000;
- 2. Urheim S , Edvardsen T , Torp H , Angelsen B , Smiseth OA Myocardial strain by Doppler echocardiography. Validation of a new method to quantify regional myocardial function. Circulation. 102: 1158- 64 2000;
- 3. Heimdal A , Stoylen A , Torp H , Skjaerpe T Real-time strain rate imaging of the left ventricle by ultrasound. Journal of the American Society of Echocardiography. 11: 1013- 9 1998;
- 4. Donal E , Raud-Raynier P , Coisne D , Allal J , Herpin D Tissue Doppler echocardiographic quantification. Comparison to coronary angiography results in Acute Coronary Syndrome patients. Cardiovascular Ultrasound vol. 3: 10- 2005;
- 5. Kukulski T , Jamal F , Herbots L , D'Hooge J , Bijnens B , Hatle L , De Scheerder I , Sutherland GR Identification of acutely ischemic myocardium using ultrasonic strain measurements. A clinical study in patients undergoing coronary angioplasty. Journal of the American College of Cardiology. 41: 810- 9 2003;
- 6. Edvardsen T , Gerber BL , Garot J , Bluemke DA , Lima JA , Smiseth OA Quantitative assessment of intrinsic regional myocardial deformation by Doppler strain rate echocardiography in humans: validation against three-dimensional tagged magnetic resonance imaging. Circulation. 106: 50- 6 2002;
- 7. Claessens P , Claessens C , Claessens J , Claessens M Strain Imaging: Key to the Specific Left Ventricular Diastolic Properties in Endurance Trained Athletes. Journal of Clinical and Basic Cardiology. 6: 35- 40 2003;
- 8. Guarini M , Urzua J , Cipriano A , Gonzalez W Estimation of cardiac function from computer analysis of the arterial pressure waveform. IEEE Transactions on Biomedical Engineering. 45: 1420- 8 1998;
- 9. Palladino JL , Noordergraaf A A paradigm for quantifying ventricular contraction. Cellular and Molecular Biology Letters. 7: 331- 5 2002;
- 10. Hodgkin AL , Huxley AF A quantitative description of membrane current and its application to conduction and excitation in nerve. Journal of Physiology. 117: 500- 44 1952;
- 11. Beeler GW , Reuter H Reconstruction of the action potential of ventricular myocardial fibres. Journal of Physiology. 268: 177- 210 1977;
- 12. Luo CH , Rudy Y A dynamic model of the cardiac ventricular action potential. II. Afterdepolarizations, triggered activity, and potentiation. Circulation Research. 74: 1097 - 113 1994;
- 13. Winslow RL , Rice J , Jafri S , Marban E , O'Rourke B Mechanisms of altered excitation-contraction coupling in canine tachycardia-induced heart failure, II: model studies. Circulation Research. 84: 571- 86 1999;
- 14. FitzHugh RA Impulses and physiological states in theoretical models of nerve membrane. Biophysical Journal. 1: 445- 466 1961;
- 15. Bardou AL , Auger PM , Birkui PJ , Chasse JL Modeling of cardiac electrophysiological mechanisms: from action potential genesis to its propagation in myocardium. Critical Reviews™ in Biomedical Engineering. 24: 141- 221 1996;
- 16. Colli Franzone P , Pavarino LF , Taccardi B Monodomain Simulations of Excitation and Recovery in Cardiac Blocks with Intramural Heterogeneity. Funcional Imaging and Modeling of the Heart (FIMH). 267- 277 2005;
- 17. Henriquez CS , Plonsey R Simulation of propagation along a cylindrical bundle of cardiac tissue--I: Mathematical formulation. IEEE Transactions on Biomedical Engineering. 37: 850- 60 1990;
- 18. Werner CD , Sachse FB , Dossel O Electrical excitation propagation in the human heart. International Journal of Bioelectromagnetism. 2–2: 2000;
- 19. Franzone PC , Guerri L , Pennacchio M , Taccardi B Spread of excitation in 3-D models of the anisotropic cardiac tissue. II. Effects of fiber architecture and ventricular geometry. Mathematical Biosciences. 147: 131- 71 1998;
- 20. Huxley AF Muscle structure and theories of contraction. Progress biophysics and biophysical chemistry. 7: 255- 318 1957;
- 21. Rice JJ , Winslow RL , Hunter WC Comparison of putative cooperative mechanisms in cardiac muscle: length dependence and dynamic responses. American Journal of Physiology. 276: H1734- 54 1999;
- 22. Bestel J , Clément F , Sorine M A biomechanical model of muscle contraction. presented at Medical Image Computing and Computer-Assisted Intervention 2001;
- 23. Rice JJ , Jafri MS , Winslow RL Modeling short-term interval-force relations in cardiac muscle. American Journal of Physiology Heart and Circulatory Physiology. 278: H913- 31 2000;
- 24. Wong AY Myocardial mechanics: application of sliding-filament theory to isovolumic concentration of the left ventricle. Journal of Biomechanics. 6: 565- 81 1973;
- 25. Hunter PJ , McCulloch AD , ter Keurs HE Modelling the mechanical properties of cardiac muscle. Progress in Biophysics & Molecular Biology. 69: 289- 331 1998;
- 26. Bovendeerd PH , Borsje P , Arts T , van De Vosse FN Dependence of intramyocardial pressure and coronary flow on ventricular loading and contractility: a model study. Annals Biomedical Engineering. 34: 1833- 45 2006;
- 27. Kerckhoffs RC , Bovendeerd PH , Kotte JC , Prinzen FW , Smits K , Arts T Homogeneity of cardiac contraction despite physiological asynchrony of depolarization: a model study. Annals of biomedical engineering. 31: 536- 47 2003;
- 28. Humphrey JD , Strumpf RK , Yin FC Determination of a constitutive relation for passive myocardium: II. Parameter estimation. Journal of Biomechanical Engineering. 112: 340- 6 1990;
- 29. Hunter PJ Myocardial constitutive laws for continuum mechanics models of the heart. Adv Exp Med Biol. 382: 303- 18 1995;
- 30. Novak VP , Yin FC , Humphrey JD Regional mechanical properties of passive myocardium. Journal of Biomechanics. 27: 403- 12 1994;
- 31. Mirsky I Assessment of passive elastic stiffness of cardiac muscle: mathematical concepts, physiologic and clinical considerations, directions of future research. Progress In Cardiovascular Diseases. 18: 277- 308 1976;
- 32. Kerckhoffs RC , Faris OP , Bovendeerd PH , Prinzen FW , Smits K , McVeigh ER , Arts T Timing of depolarization and contraction in the paced canine left ventricle: model and experiment. Journal of Cardiovascular Electrophysiology. 14: 188- 95 2003;
- 33. May-Newman K , McCulloch AD Homogenization modeling for the mechanics of perfused myocardium. Progress in Biophysics & Molecular Biology. 69: 463- 81 1998;
- 34. Sermesant M , Moireau P , Camara O , Sainte-Marie J , Andriantsimiavona R , Cimrman R , Hill DL , Chapelle D , Razavi R Cardiac function estimation from MRI using a heart model and data assimilation: advances and difficulties. Medical Image Anals. 10: 642- 56 2006;
- 35. Vetter FJ , McCulloch AD Three-dimensional stress and strain in passive rabbit left ventricle: a model study. annals of biomedical engineering. 28: 781- 92 2000;
- 36. Mohr MBBLG , Seemann G , Sachse FB , Dössel O Volume Modeling of Myocard Deformation with a Spring Mass System. Lecture Notes in Computer Science. 2673: 332- 339 2003;
- 37. Chahboune B , Crolet JM Numerical simulation of the blood-wall interaction in the human left ventricle. European Physical Journal. 2: 291- 297 1998;
- 38. Verdonck PR , Vierendeels JA Fluid-Structure Interaction Modelling of Left Ventricular Filling. International Conference on Computational Science. 275 - 284 2002;
- 39. Sermesant M , Delingette H , Ayache N An electromechanical model of the heart for image analysis and simulation. ieee transactions on medical imaging. 25: 612- 25 2006;
- 40. Kerckhoffs RC , Neal ML , Gu Q , Bassingthwaighte JB , Omens JH , McCulloch AD Coupling of a 3D finite element model of cardiac ventricular mechanics to lumped systems models of the systemic and pulmonic circulation. annals of biomedical engineering. 35: 1- 18 2007;
- 41. Courtois M , Kovacs SJ Jr , Ludbrook PA Transmitral pressure-flow velocity relation. Importance of regional pressure gradients in the left ventricle during diastole. Circulation. 78: 661- 71 1988;
- 42. Nickerson D , Smith N , Hunter P New developments in a strongly coupled cardiac electromechanical model. Europace. 7: (Suppl 2, pp) 118- 27 2005;
- 43. Ubbink SW , Bovendeerd PH , Delhaas T , Arts T , van de Vosse FN Towards model-based analysis of cardiac MR tagging data: relation between left ventricular shear strain and myofiber orientation. Medical Image Anals. 10: 632- 41 2006;

- 44. Desaive T , Ghuysen A , Lambermont B , Kolh P , Dauby PC , Starfinger C , Hann CE , Chase JG , Shaw GM Study of ventricular interaction during pulmonary embolism using clinical identification in a minimum cardiovascular system model. presented at Conference of the IEEE Engineering in Medicine and Biology (EMB) Lyon France 2007;
- 45. Silva CE , Ferreira LD , Peixoto LB , Monaco CG , Gil MA , Ortiz J Study of the myocardial contraction and relaxation velocities through Doppler tissue imaging echocardiography: A new alternative in the assessment of the segmental ventricular function. Arquivos Brasileiros de Cardiologia. 78: 200- 11 2002;
- 46. Cerqueira MD , Weissman NJ , Dilsizian V , Jacobs AK , Kaul S , Laskey WK , Pennell DJ , Rumberger JA , Ryan T , Verani MS Standardized myocardial segmentation and nomenclature for tomographic imaging of the heart. A statement for healthcare professionals from the Cardiac Imaging Committee of the Council on Clinical Cardiology of the American Heart Association. International Journal of Cardiovascular Imaging. 18: 539- 42 2002;
- 47. Szathmary V , Osvald R An interactive computer model of propagated activation with analytically defined geometry of ventricles. Comput Biomed Res. 27: 27- 38 1994;
- 48. Taber LA , Yang M , Podszus WW Mechanics of ventricular torsion. Journal of Biomechanics. 29: 745- 52 1996;
- 49. Hernandez AI Fusion de signaux et de modèles pour la caractérisation d'arythmies cardiaques. thesis of Rennes university. France 2000;
- 50. Hernandez AI , Carrault G , Mora F , Bardou A Model-based interpretation of cardiac beats by evolutionary algorithms: signal and model interaction. Artificial Intelligence in Medicine. 26: 211- 35 2002;
- 51. Durrer D , van Dam RT , Freud GE , Janse MJ , Meijler FL , Arzbaecher RC Total excitation of the isolated human heart. Circulation. 41: 899- 912 1970;
- 52. Chaudhry HRB , Findley T Stresses and Strains in the Passive Left Ventricle. Journal of Biological Systems. 4: 535- 554 1996;
- 53. Back L Left ventricular wall and fluid dynamics of cardiac contraction. Mathematical Biosciences. 36: 257 - 297 1977;
- 54. Takata M , Harasawa Y , Beloucif S , Robotham JL Coupled vs. uncoupled pericardial constraint: effects on cardiac chamber interactions. Journal of Applied Physiology. 83: 1799- 813 1997;
- 55. Ursino M , Magosso E Acute cardiovascular response to isocapnic hypoxia. I. A mathematical model. American Journal of Physiology Heart and Circulatory Physiology. 279: H149- 65 2000;
- 56. Wendling F , Hernandez AI , Bellanger J-J , Chauvel P , Bartolomei F Interictal to Ictal Transition in Human Temporal Lobe Epilepsy: Insights From a Computational Model of Intracerebral EEG. Journal of Clinical Neurophysiology. 22: 343- 356 2005;
- 57. Streeter DD Jr , Hanna WT Engineering mechanics for successive states in canine left ventricular myocardium. I. Cavity and wall geometry. Circulation Research. 33: 639- 55 1973;
- 58. Holland JH Adaptation in natural and artificial systems. MIT press; 1975;
- 59. Beasley D , Bull DR , Martin R An overview of genetic algorithm: Part1, Fundamental. Univ Comp. 15: 170- 181 1993;
- 60. Goldberg DE Genetic Algorithms in search, optimization and machine learning. Boston Kluwer Academic Publishers; 1989;
- 61. Michalewicz Z Genetic Algorithms + Data Structures = Evolution Programs. New-York Springer-Verlag; 1994;
- 62. Bookstein FL Principal Warps: Thin-Plate Splines and the Decomposition of Deformations. IEEE trans Pattern Analysis and Machine Intelligence. 11: 567- 585 1989;
- 63. Yu CM , Gorcsan J 3rd , Bleeker GB , Zhang Q , Schalij MJ , Suffoletto MS , Fung JW , Schwartzman D , Chan YS , Tanabe M , Bax JJ Usefulness of tissue Doppler velocity and strain dyssynchrony for predicting left ventricular reverse remodeling response after cardiac resynchronization therapy. American Journal of Cardiology. 100: 1263- 70 2007;
- 64. Beshai J , Grimm RA , Nagueh SF , Baker JH , Beau SL , Greenberg SM , Pires LA , Tchou PJ Cardiac-Resynchronization Therapy in Heart Failure with Narrow QRS Complexes. New England Journal of medicine vol. 357: 2461- 2471 2007;
- 65. Dauterman K , Pak PH , Maughan WL , Nussbacher A , Arie S , Liu CP , Kass DA Contribution of external forces to left ventricular diastolic pressure. Implications for the clinical use of the Starling law. Annals of Internal Medicine. 122: 737- 42 1995;

Figure 1

1) Tissue Doppler Imaging applied to a four-cavity echocardiographic acquisition. 2) A typical experimental strain of a segment can be divided in several phases: isovolumic contraction (IC), ejection (S), isovolumic relaxation (IR), rapid filling (RF), slow filling period (SF) and atrial systole (A)

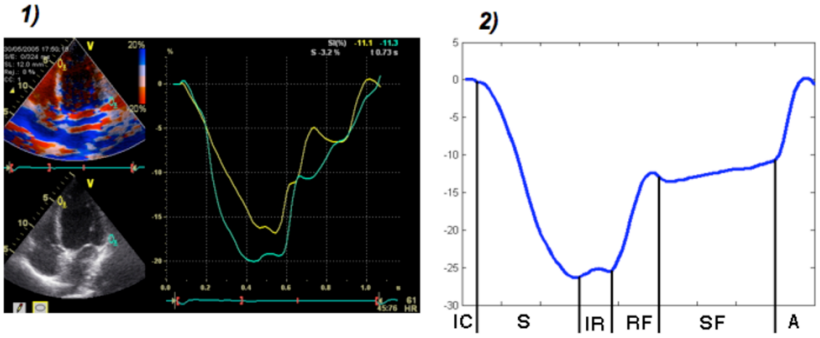

Figure 2

Ventricular model segmentation. The model is composed of 12 segments, corresponding to the septal, lateral, anterior and inferior components for three different layers (basal, equatorial and apical). This graphical representation will be used in figure 12.

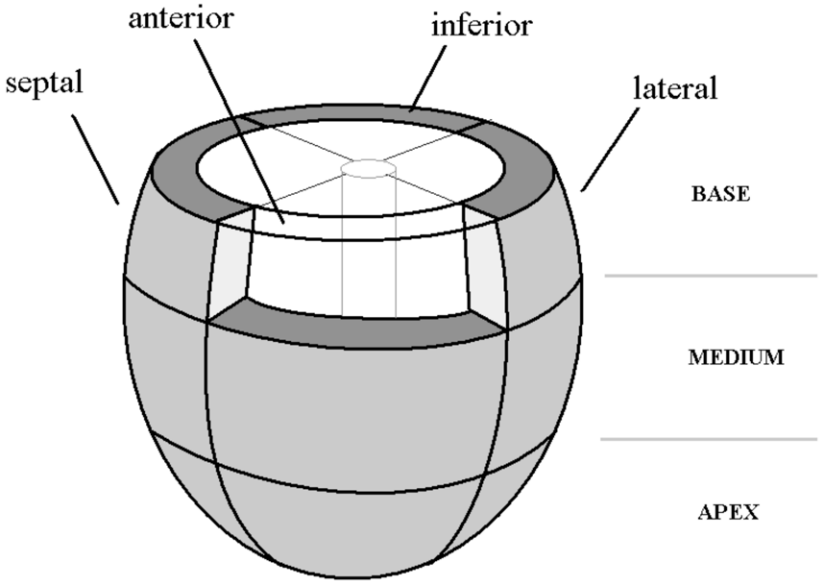

Figure 3

States and coupling conditions for cellular automata models. Each automaton is characterized by four electrical states: i) rapid depolarization period (RDP), ii) absolute refractory period (ARP), iii) relative refractory period (RRP) and iv) a waiting period (idle).

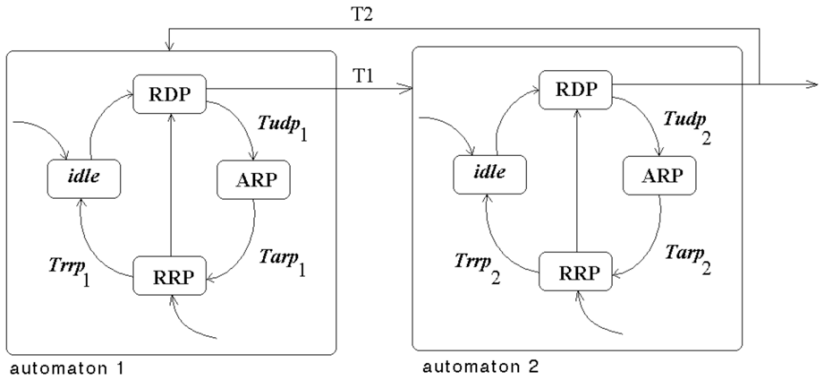

Figure 4

Model of each ventricular segment. The mechanical model is connected to the electrical model and the mechano-hydraulic coupling entity respectively through a simplified calcium concentration ([Ca2+]) representation, the radial force (F) and velocity (dr/dt). The hydraulic model is linked to the mechano-hydraulic coupling entity and to the other segments respectively through the wall surface pressure (Ps), the flow (Q), and the pressure at the center of the cavity (Pc).

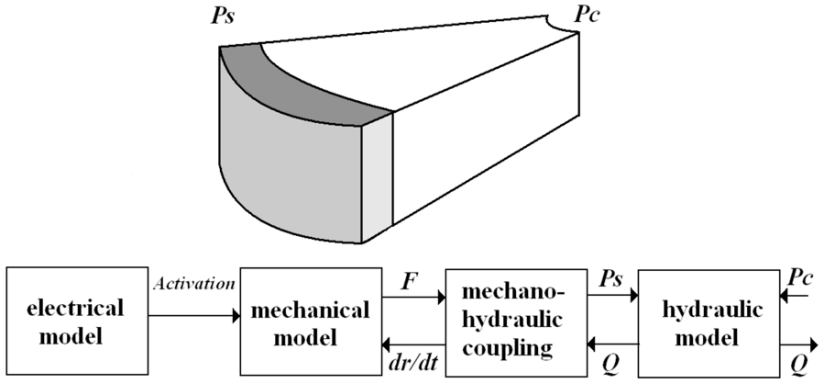

Figure 5

The twelve segments are connected in the hydraulic domain by adding each segment's flow and by supposing that the pressures are equal at the center of each layer.

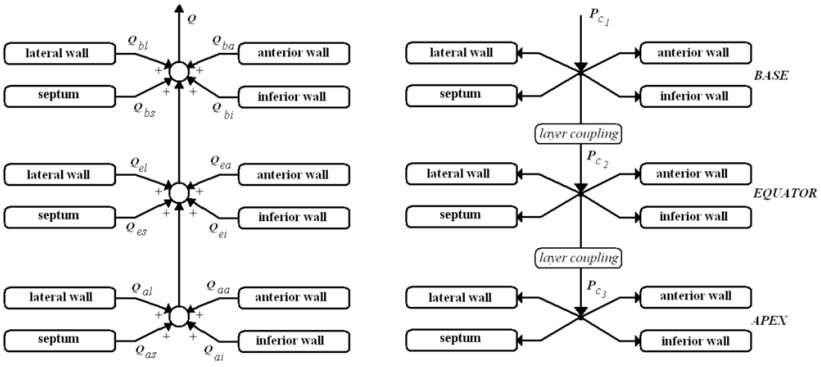

Figure 6

I) Stable resting left ventricular pressure-volume loop acquired from a human. The figure has been reproduced with permission from [65], II) Model simulation of ventricular hemodynamic variables for one beat: A) intra-ventricular pressure B) aortic flow C) volume D) pressure-volume loop.

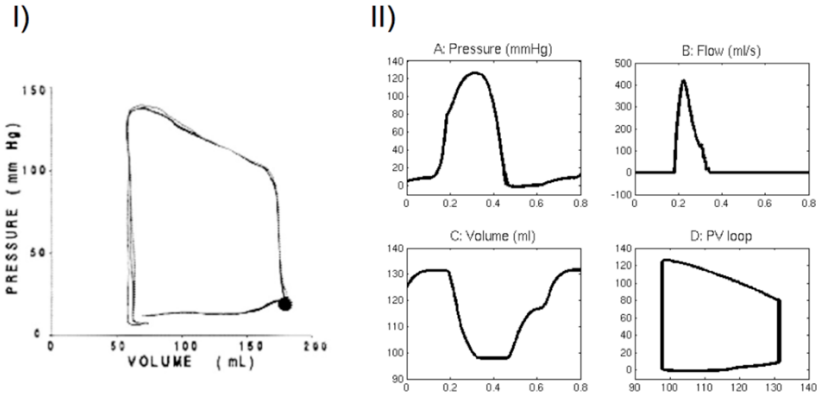

Figure 7

Strain simulation in healthy (left panel) and pathologic (right panel) conditions. The pathologic case was simulated by applying an electrical activation delay of 50 ms on the anterior basal segment. The extension of the delayed segment can be observed for the pathologic case during the isovolumic contraction phase (marked with a circle).

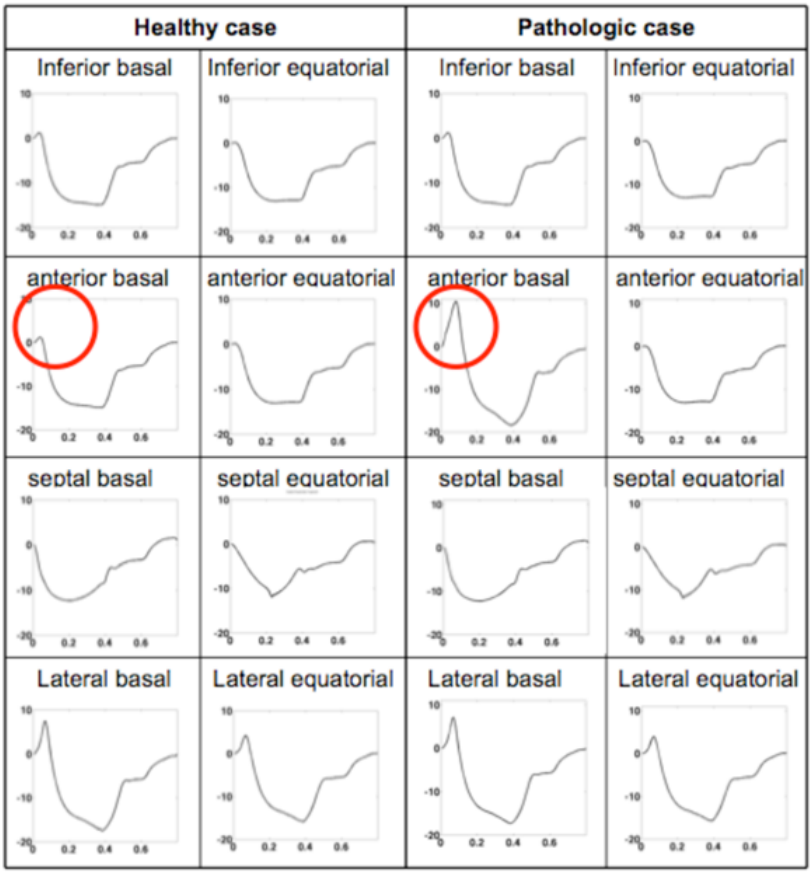

Figure 8

Parameters adaptation process. The evaluation of the error between observable signals and simulations is minimized in order to determine the model's parameters using an identification algorithm. The parameter values are representative of the physiological system state and can help to interpret observations.

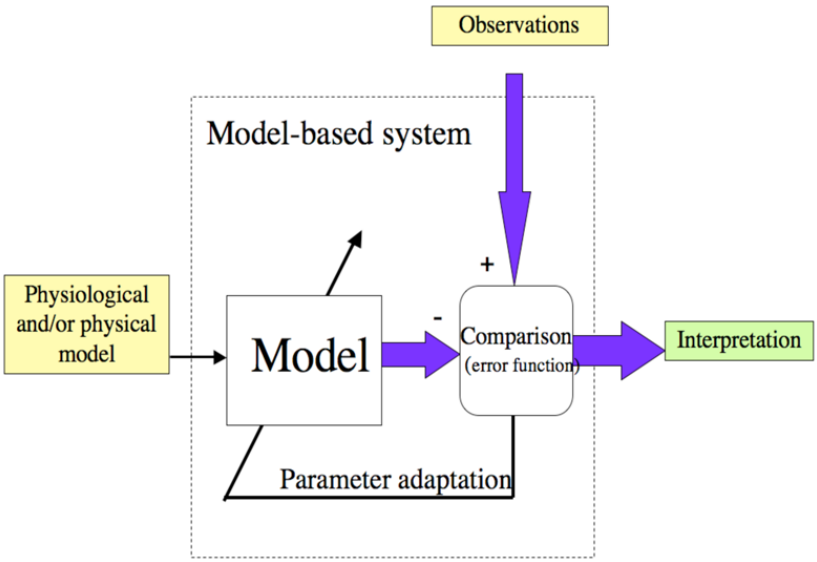

Figure 9

Ellipsoidal model dimensions obtained from echocardiographic measures: a and b are respectively the minor and major axis sizes.

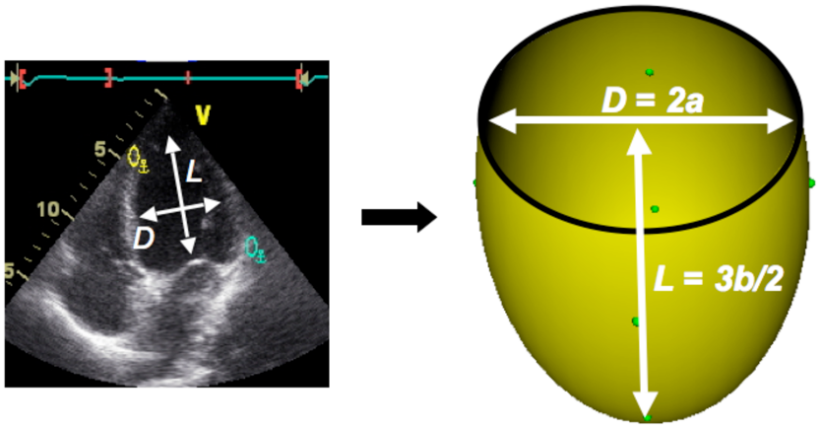

Figure 10

Working principles of evolutionary algorithms. A population is firstly initialized. The iterative procedure includes the evaluation of the error function, individual selection and the creation of a new population using genetic operators. The process is applied until it reaches the stopping criteria.

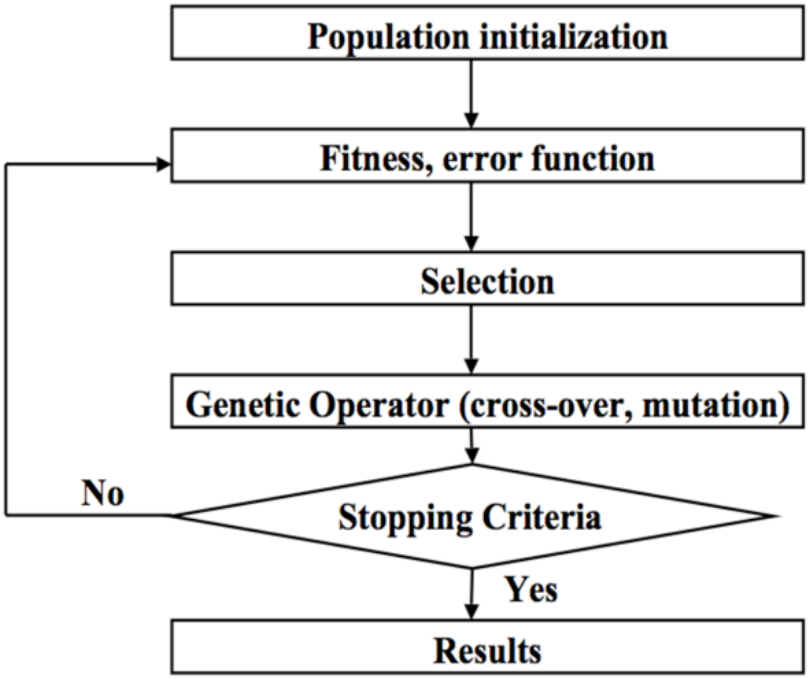

Figure 11

Comparison between simulated and experimental strains for the two healthy subjects and the pathologic patient during one cardiac cycle for the septum, anterior, inferior and lateral walls of the base and equator. The continuous curve is the simulation and the segmented one is the experimental data. The strain is expressed as a percentage of the diastolic state.

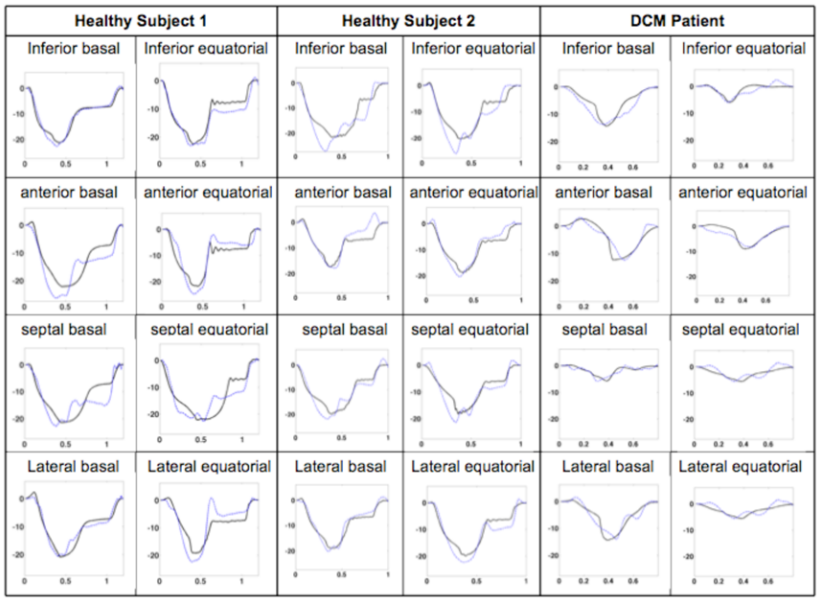

Figure 12

Contraction of the electromechanical model for the two healthy subjects and the pathologic patient. The color legend corresponds to the electrical state of each segment and is expressed in mV. The orientation of the ventricular model is depicted in the lower right panel of the figure.

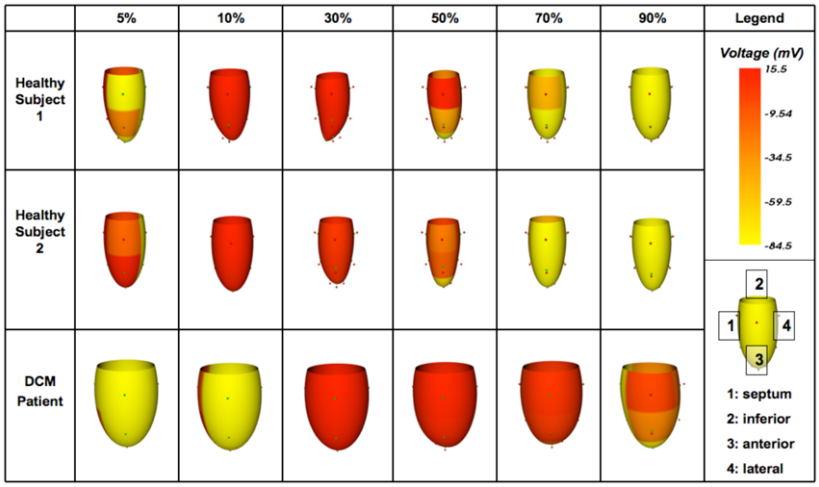

Figure 13

Bull's eye representation of ventricular parameters. For each Bull's eye diagram, the left, top, right and down parts represent the septal, anterior free wall and posterior regions, respectively. The outer, mid- and inner rings represent the base, the equator and the apex of the LV. This representation will be used in figures 14 and 15.

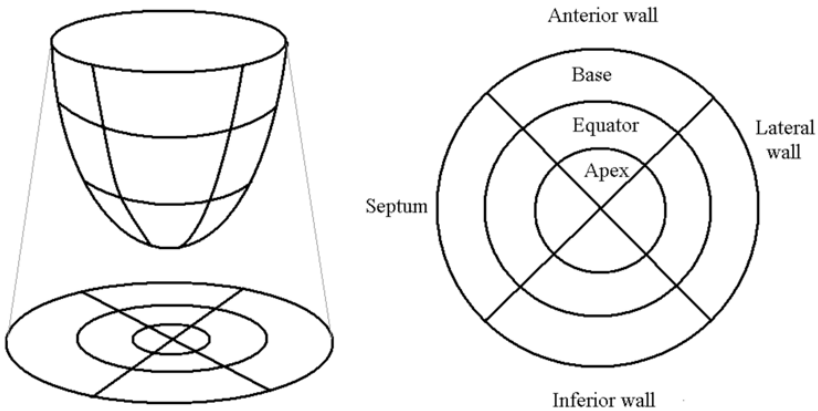

Figure 14

Bull's eye representation of the electrical activation times (TAE) for the two healthy subjects and the pathologic patient. The maximum values reach 54 ms, 67.4 ms and 126 ms respectively for the first, second subject and the pathologic patient.

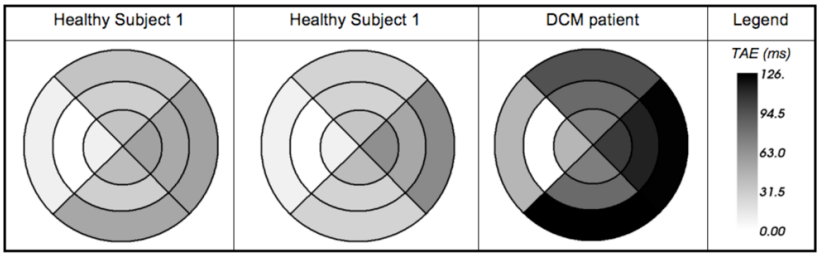

Figure 15

Bull's eye representation of the mechanical activity peak time expressed as a percentage of the RR-interval (TMP%) for the two healthy subjects and the pathologic patient. These values are high for the anterior and lateral segments of the DCM patient.

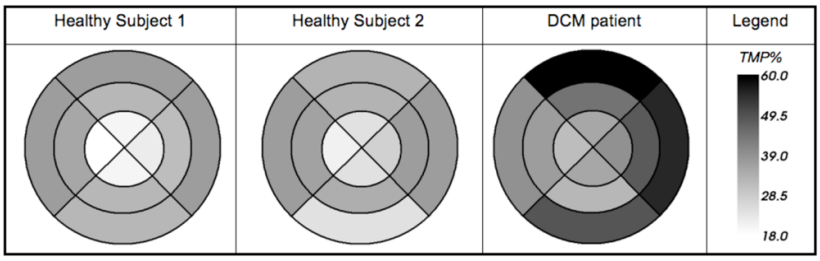

Figure 16

The identification algorithm has been repeated ten times on one subject in order to test the robustness of the identified parameters. This figure shows the boxplot of the ten identified T_{MP} for the first healthy subject.

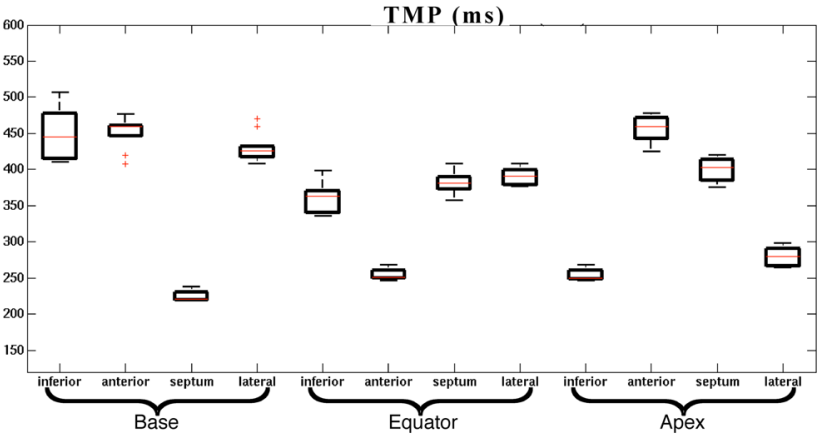

Table 1
Minor (a) and major (b) axis values for the three patients.

	Healthy	Healthy	DCM
minor axis a	1.9725	1.8575	3.22
major axis b	4.8067	4.8033	5.99

Table 2
Model parameter values.

C5	Parameters Values 141 mmHg	Source [10]
Preload		
Sf	25ml/s	Estimated
Atria		
Emin	1.2mmHg/ml	[56]
Emax	0.06 mmHg/ml	[56]
T	0.12s	[56]
Afterload		
R	3 mmHg.s/ml	[24]
C	0.219 ml/mmHg	[40]
I	0.00082 mmHg.s2/ml	[40]
Valve		
Rpass	0.01 mmHg.s/ml	Estimated
Rblo	100 mmHg.s/ml	Estimated
VENTRICLE		
Valvular Plan		
C	0.05 ml/mmHg	Estimated
Hydraulic Résistance		
T1	0.03s	Estimated
T2	0.05*RR s	Estimated
Inertance		
I	0.0001 mmHg.s2/ml	Estimated
Geometric Parameters		
Mean fibre angle with respect to the equatorial plane	π/12	[52]
Thickness	1 cm	[52]
Active Properties		
Tref	940 mmHg	[32]
B0	1.45	[32]
B1	1.95	[32]

n_ref	4.25	[32]
pC50_ref	5.33	[32]
B2	0.31	[32]
Passive Properties		
C1	113.9 mmHg	[10]
C2	550.71 mmHg	[10]
C3	10.5 mmHg	[10]
C4	−146.1 mmHg	[10]